

Two-dimensional crystalization on spheres: Crystals grow cracked

Laureano Ortellado , Daniel A. Vega, and Leopoldo R. Gómez ^{*}

Department of Physics, Universidad Nacional del Sur-IFISUR-CONICET, Av. Alem 1253, Bahía Blanca, Argentina



(Received 22 September 2021; accepted 3 January 2022; published 13 January 2022)

Here we study how curvature affects the structure of two-dimensional crystals growing on spheres. The mechanism of crystal growth is described by means of a Landau model in curved space that accounts for the excess of strain on crystal bonds caused by the substrate's curvature (packing frustration). In curved space elastic energy penalization strongly dictates the geometry of growing crystals. While compact faceted crystals are observed when elastic energy contribution can be neglected, cracked crystals with ribbonlike forms appear as the main mechanisms to reduce elastic frustration for highly curved systems.

DOI: [10.1103/PhysRevE.105.014801](https://doi.org/10.1103/PhysRevE.105.014801)

I. INTRODUCTION

The growth of a two-dimensional (2D) crystal layer on a planar substrate is dictated by the competition between an energy gain, obtained by forming a piece of the equilibrium crystal, and a line tension penalty due to the interface of the nuclei with the surroundings [1,2]. This free-energy competition produces a critical size for crystal growth. Only those nuclei overcoming this critical size can grow by adding crystal particles to their surface. Sub-critical nuclei collapse by surface tension. In addition to this simple mean-field description of the nucleation and growth, some complexities may arise from different energy exchange mechanisms, limited particle's diffusion, and anisotropic nuclei line tension, between other effects, which can lead to a variety of dynamics and nuclei shapes [1,2].

On the contrary, it could be simply impossible to grow a perfect crystal on a curved substrate [3]. This is because the underlying curvature may induce distortions of the crystal lattice, increasing its strain energy (an effect known as geometric frustration) [4,5]. In this sense, depending on the underlying geometry, a crystal may need to be highly deformed to wrap on the curved surface, increasing thus the elastic energy of the lattice structure. For example, the free energy of a perfect circular crystal of size R growing on a sphere of radius a (spherical cap) has been modeled through the free energy [6,7]:

$$\Delta F_{\text{cap}} = 2\pi R\gamma - \pi|\Delta f|R^2 + \frac{\pi}{384}Y\frac{R^6}{a^4}, \quad (1)$$

where Y is the two-dimensional Young's modulus of the crystal, Δf is the energy difference between crystal and melt, and γ is the line tension of the interface between the two regions.

In this equation, the first two terms represent the competition between surface and line tension energies discussed above. The last term is a free-energy penalization induced by the substrate's nonplanar geometry, which inhibits fur-

ther growth of the nuclei beyond the equilibrium size $R_{\text{eq}} \sim (\Delta f/Y)^{\frac{1}{4}}a$ [7]. In a planar domain, it is also possible to frustrate a crystal under stress if the intrinsic curvature is associated with the interactions of the particles [8].

However, growing nuclei on curved surfaces could reduce the elastic frustration in two ways. One possibility is by the inclusion of topological defects while growing [9,10]. This is because topological defects can contribute to reducing elastic distortions on the lattice, allowing further propagation. The other possibility is by changing the shape of the crystal to ribbonlike or ramified structures, which has been recently observed in experiments with colloidal crystals growing in spheres [7], in Monte Carlo simulations of self-assembly of viral capsids [11], and phase field simulations [12,13].

In this work, we study the process of isothermal crystallization on spherical substrates by using a free-energy functional which takes into account the elastic stress induced by geometric frustration. We show that elastic stress dictates the growth pathway. Growing crystals may change their shape and also crack, depending on the substrate's curvature and lattice rigidity.

II. MODEL

In Landau's theory of phase transitions, the free-energy functional of the system is expanded in terms of an appropriate order parameter $\Phi(\mathbf{r})$, which is mainly related to the underlying symmetries of the system [14]. In studies of crystallization, the complex order parameter Φ is commonly chosen as scalar function representing the local density and orientation of the material, and the dynamics of the phase transition can be studied through a relaxational equation of the form [15]

$$\frac{\partial \Phi}{\partial t} = -\mu \frac{\delta F}{\delta \Phi}, \quad (2)$$

where μ is the mobility coefficient of the system, F depends on the details of the system studied, and $\delta F/\delta \Phi$ is the functional derivative of F in terms of the complex order parameter Φ .

^{*}lgomez@uns.edu.ar

In this work, we study crystallization on curved surfaces by using a complex order parameter $\Phi(\mathbf{r}) = \phi(\mathbf{r})e^{i\Theta(\mathbf{r})}$. The parameter field ϕ (hereafter, order parameter) is a measure of the degree of local order in the system during the phase transition. Its values range from 0, when the system is locally fully disordered in the liquid phase, to 1 when the system is locally fully ordered in a crystalline phase. The phase $\Theta(\mathbf{r})$ defines the local orientation of the crystal which takes values over the range of $-\pi$ to π . Crystals have a N -fold symmetry C_N that restricts the domain of Θ to lie in the irreducible range $-\pi/N < \Theta \leq \pi/N$ [16,17].

Points on the surface of the substrate are specified by curvilinear coordinates $\mathbf{r} = (x_1, x_2)$; therefore, the metric of the surface takes the form $ds^2 = g_{ij}dx^i dx^j$, where g_{ij} is the metric tensor [18]. In the plane, the lattice orientation can be defined as the angle between a crystallographic direction and a unit basis vector corresponding to a particular axis. The same notion can be applied to curvilinear coordinates. Note, however, that as in general the unit basis vector orientations are functions of the local position, the relative orientation between the crystal and the bases vector changes. Thus, in non-Euclidean spaces, at different positions physically equivalent crystallographic directions result in different crystallographic orientations [17].

Here we use a variation of the Kobayashi-Warren-Carter (KWC) model, which can be used to study crystallization on curved geometries. This model has been widely used to study isothermal grain growth and grain boundary formation and evolution [16,17,19,20] in both 2D and 3D Euclidean systems and in planar conical systems [17]. The KWC model is composed on an interfacial energy $F_I = \int e(\nabla\phi, \Theta)|\nabla\phi|^2 dS$, bulk energy $F_B = \int f(\phi)dS$, and elastic energy $F_E = \int (s_0\phi^2|\nabla\Theta - \mathbf{\Lambda}| + t_0\phi^2|\Theta - \mathbf{\Lambda}|^2)dS$.

The total free-energy functional in the KWC model is given by

$$F = \int \{e(\nabla\phi, \Theta)|\nabla\phi|^2 + f(\phi) + s_0\phi^2|\nabla\Theta - \mathbf{\Lambda}| + t_0\phi^2|\Theta - \mathbf{\Lambda}|^2\} dS. \quad (3)$$

On curved geometries, the gradient and surface element are written in curvilinear coordinates as $\nabla = g^{ij}\partial_j$, where $g^{ij} = (g^{-1})_{ij}$, g is the determinant of the metric tensor and $\frac{\partial}{\partial x_i} = \partial_i$, and $dS = \sqrt{g} dx_1 dx_2$.

Note that in this expression the gradient for the crystal orientation Θ is $\nabla\Theta \rightarrow \nabla\Theta - \mathbf{\Lambda}$, where $\mathbf{\Lambda}$ is the spin-connection which takes into account the space variation of basis vectors due to the non-Euclidean geometry. The spin-connection can be viewed as the ‘‘geometric vector potential,’’ since the curl of the spin-connection is the Gaussian curvature $\nabla \times \mathbf{\Lambda}(\mathbf{r}) = G(\mathbf{r})\hat{n}$ in the same way as the curl of the electromagnetic vector potential \mathbf{A} is the magnetic field $\nabla \times \mathbf{A}(\mathbf{r}) = \mathbf{B}(\mathbf{r})$, where \hat{n} is the surface normal.

In the free-energy functional Eq. (3) $f(\phi)$ represents the local free energy of an homogeneous system having an order parameter ϕ . Within the frame of the Ginzburg-Landau theories of phase transitions, this free-energy contribution is considered as a polynomial expansion in terms of the order parameter ϕ . This approach has been extensively used in the literature to describe a wide diversity of crystal forming

systems, ranging from self-assembling soft block copolymer hexagonal patterns up to hard-crystals (see, for example, Refs. [10,21–23] and references therein).

To model first order phase transitions $f(\phi)$ needs to have the form of an asymmetrical double-well potential, where each local minimum represents one of the equilibrium phases (the local minimum of highest energy is located at the initial disordered state $\phi = 0$, and the other absolute minimum is located at the final crystal state $\phi = 1$) [21]:

$$f(\phi) = \frac{w}{4}\phi^4 - \left(\frac{w}{2} - \frac{m}{3}\right)\phi^3 + \left(\frac{w}{4} - \frac{m}{2}\right)\phi^2, \quad (4)$$

where the parameter m controls the driving force to the crystal phase and w controls the strength of the double-well barrier. For adiabatic crystal growth, m is a function of the temperature [24]. In this work we consider an isothermic growth, therefore, m is a constant. To facilitate the crystal growth we set $m = 0.5$, i.e., we set the temperature of the system where $f(\phi)$ becomes a single-well potential with an inflection point at $\phi = 0$. The parameter w controls the height of the activation barrier between the two phases at the melting temperature. Therefore, this sets the interface width W , by the relation $W \sim \sqrt{\frac{\epsilon}{w}}$ [20]. In addition, w is a measure of the latent heat per area of solidification. Here we have also set $w = 1$.

The term $e(\nabla\phi, \Theta)$ in Eq. (3) represents the penalization to form interfaces. In the specific case of a liquid-solid interface, the parameter $e(\nabla\phi, \Theta)$ represents the surface tension of the crystal that depends on the crystal orientation. In curvilinear coordinates, the crystal orientation is defined by the angle ψ that the crystal growth front ($-\nabla\phi$) makes with the \hat{x}_1 versor, i.e., $\tan(\psi) = \left(\frac{-\partial_x \phi / \sqrt{g_{22}}}{-\partial_{x_1} \phi / \sqrt{g_{11}}}\right)$. It can also be defined as the relative orientation α that is the difference of ψ with the orientational map Θ , thus,

$$\alpha = \psi - \Theta. \quad (5)$$

For crystals having N -fold symmetry, this needs to be reduced to principal domain $[-\frac{\pi}{n}, \frac{\pi}{n})$. Taking this into account, the $e(\alpha)$ parameter can be defined as

$$e(\alpha) = \frac{1}{2}\{e_0[1 + \delta_0 \cos(n\alpha)]\}^2, \quad (6)$$

where e_0 controls the magnitude of line tension penalization, n represents the N -fold symmetry C_N of the system ($n = 4$ for a square, $n = 6$ for a hexagon, and so on), and δ_0 controls the strength of the anisotropy.

The third and fourth terms in the free-energy functional in Eq. (3) ensure the formation and motion of stable grain boundaries of finite width, respectively [16,17]. The coefficients are written such that variations in the lattice orientation are penalized for a well-ordered phase. The fourth term in the free-energy functional, related to the motion of grain boundaries, is needed in the case of studies concerning the long-time grain growth and coarsening in polycrystalline systems. Here, for simplicity, we consider the case $t_0 = 0$. As expected, we have found similar numerical results for the growth of a single crystal seed on a sphere for $t_0 \neq 0$.

For the KWC model, the relaxational equations which describe the dynamics of the phase transition take the

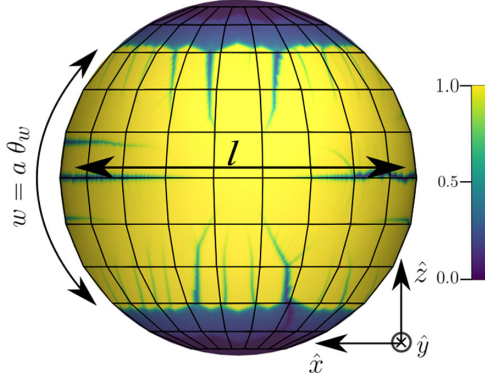


FIG. 1. Spherical crystal and geometric parameters describing its shape. This figure shows the computational grid used to solve the equation in spherical coordinates. The parameters l and w represent the length and the width of the ribbonlike crystal cap, respectively.

form:

$$\begin{aligned} \mu_\phi \frac{\partial \phi}{\partial t} &= -\frac{\delta F}{\delta \phi}, \\ \mu_\Theta \frac{\partial \Theta}{\partial t} &= -\frac{\delta F}{\delta \Theta}, \end{aligned} \quad (7)$$

where μ_ϕ and μ_Θ are the kinetic scaling factors of the system. Defining the free energy F as $F = \int L(\phi, \nabla \phi, \Theta, \nabla \Theta) dS$, the functional derivatives are written

$$\begin{aligned} \frac{\delta F}{\delta \phi} &= \frac{\partial L}{\partial \phi} - \nabla \cdot \left(\frac{\partial L}{\partial \nabla \phi} \right), \\ \frac{\delta F}{\delta \Theta} &= \frac{\partial L}{\partial \Theta} - \nabla \cdot \left(\frac{\partial L}{\partial \nabla \Theta} \right), \end{aligned} \quad (8)$$

where the divergence operator in curvilinear coordinates is written $\nabla \cdot = \frac{1}{\sqrt{g}} \partial_i \sqrt{g}$.

For the KWC model these derivatives take the form

$$\begin{aligned} \frac{\delta F}{\delta \phi} &= - \left[2 \nabla e(\alpha) \cdot \nabla \phi + 2e(\alpha) \nabla^2 \phi + e'(\alpha) \frac{\partial \alpha}{\partial \nabla \phi} |\nabla \phi|^2 \right] \\ &\quad + f'(\phi) + 2s_0 \phi |\nabla \Theta - \Lambda|, \\ \frac{\delta F}{\delta \Theta} &= - \nabla \cdot \left[s_0 \phi^2 \frac{\nabla \Theta - \Lambda}{|\nabla \Theta - \Lambda|} \right] + e'(\phi) \frac{\partial \alpha}{\partial \Theta} |\nabla \phi|^2. \end{aligned} \quad (9)$$

To study isothermal crystal growth on spheres we write the equations in spherical coordinates, where points on the sphere are specified by $\mathbf{r}(\theta, \varphi)$, where $x_1 = \theta \in [0, \pi]$ is the polar angle measured from a fixed zenith direction, and $x_2 = \varphi \in [0, 2\pi)$ is the azimuth angle (Fig. 1). In these coordinates, the surface element ds is given by $ds^2 \equiv |d\mathbf{r}|^2 = a^2 d\theta^2 + \sin^2(\theta) a^2 d\varphi^2$. The evolution equations are numerically solved in Python using a finite-difference scheme, forward in time and centered in space. As mentioned earlier, the local orientation of the lattice is defined as the angle between the crystallographic direction and a unit basis vector. Here, for simplicity, the orientation is measured with respect to the latitudinal axis using the unit basis vector $\hat{\theta}$. As the initial crystal seed, we use a small spherical cap having $\phi = 1$, and we set $\phi = 0$ on the rest of the sphere [25]. Multiple growing nuclei can be modeled by seeding on different parts of the sphere. The time position of the interface is identified here as the

region where the order parameter takes its intermediate value $\phi = 0.5$. For the initial orientational field Θ , we use a constant orientation inside the crystal seed, and a random phase for the rest of the sphere. Typically, we set the parameters $e_0 = 0.01$, $\mu_\phi = 3 \times 10^{-4}$, $\mu_\Theta = 3 \times 10^{-5}$, and $\delta_0 = 0.2$, as used in other numerical studies [16,24]. Due to the spherical coordinates, our computational grid is not uniform and the cell size decreases in the polar angle direction until it reaches a maximum at the equator of the sphere, as can be seen from Fig. 1. At the pole of the sphere, the element size is zero, and hence the pole is a singular point. However, due to the geometric frustration, for the systems studied here the crystallization is completed without reaching the poles, even for the cases where the crystal rigidity is small ($s_0 \sim 0.01$). To use equivalent grids, we vary the number of grid points for the different spheres (from $n_\theta \times n_\varphi = 200 \times 400$ for spheres of $a = 1.5$, to $n_\theta \times n_\varphi = 466 \times 932$ for spheres of $a = 3.5$). The angular steps are given by $\Delta\theta = \frac{\pi}{n_\theta - 1}$ and $\Delta\varphi = \frac{2\pi}{n_\varphi - 1}$.

III. RESULTS

Figure 2 shows the growth of an initial circular nucleus on a spherical substrate of radius $a = 1.5$. Here time flows from left to right, and the top and bottom rows correspond to the order parameter ϕ and the crystal orientation Θ maps, respectively. In the Supplemental Material, movies show the growth of the crystal on the surface of the sphere (movie 1), and as seen through a Mercator projection (movie 2) [26].

From this figure, it is clear that the underlying curvature largely modifies the process of crystal growth on spherical substrates. As the nucleus is growing, the substrate's curvature induces a continuous change in the lattice orientation (see the first two figures on the bottom row). This variation in the lattice orientation produces a large increment in the elastic energy, which inhibits further isotropic growth. Here, to continue its growth, the nucleus cracks in pieces of approximately constant orientation (last two columns). Note that while domain walls can be identified with variations in the orientational field Θ , cracks can be identified with regions that failed to crystallize, such that the order parameter ϕ remains near zero, even at long times.

This is a purely geometric effect due to the curvature of the substrate. Experiments made by Mitchell *et al.*, show similar crystal patterns when nanoparticles sheets are forced to cover surfaces with positive Gaussian curvature [27].

Note that the cracks that appear here as a mechanism to relax the elastic energy are similar to the fractal-like ramification observed in spherical colloidal crystals [7]. Here, initially the nucleus grows into a sixfold crystallite and cracks appear on the faces of the hexagon which are regions under the highest tension, as it is shown in the first column of Fig. 2. A similar mechanism was observed in simulations of crystal growth on spheres, based on a different phase field model [12].

To understand the departure from isotropic growth, here we evaluate the excess of free energy by elastic frustration of a growing circular nucleus:

$$F_E = \int s_0 \phi^2 |\nabla \Theta - \Lambda| dS \approx \frac{2}{3} \pi s_0 \frac{R^3}{a^2}. \quad (10)$$

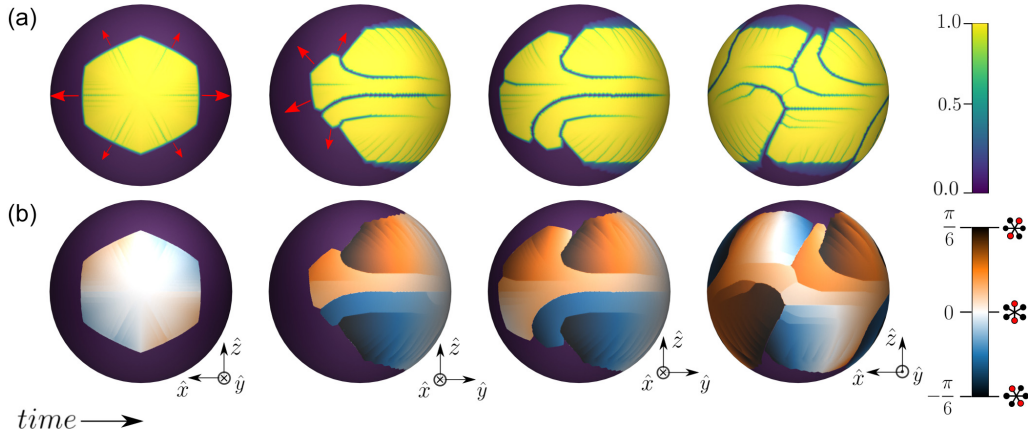


FIG. 2. Crystallization on a sphere. This figure shows the formation over time of domain walls of a rigid crystal with $s_0 = 0.05$ on a sphere of radius $a = 1.5$. The first row (a) represents the order parameter ϕ and the second row (b) represents the orientational field Θ . The first two columns represent the view from the normal axes of the initial seed; the third column represents the view of one of the sides of the crystal, and the last column represents the view from the opposite side of the initial seed.

Thus, different from Euclidean-space, here the homogeneous crystal growth is frustrated beyond an equilibrium size determined by

$$R_{\text{eq}} \approx \frac{\Delta f + \sqrt{(\Delta f)^2 - 4\gamma s_0/a^2}}{2s_0/a^2}. \quad (11)$$

Then, when the crystal reaches the size determined by R_{eq} , it cannot grow further without reducing frustration. As pointed out in the introduction, previously it has been found that geometric frustration can be alleviated via topological defects or by changing the shape of the growing crystal. As noted in Fig. 2, in this model initial isotropic nuclei eventually acquire a fractured ribbonlike shape. As the degree of frustration is dictated by the curvature and the rigidity of the crystal, it can be expected that crystal shape becomes strongly dependent on these parameters. Figure 3 shows the shape of the final fractured ribbonlike crystals for different substrates' curvature and crystal rigidity. Here, the top row [Figs. 3(a) and 3(b)] compares the effect of the substrate curvature on the shape of the crystal. Clearly, for higher curvatures (smaller spherical substrates) the crystals become more fractured and with an enhanced ribbonlike shape. Similarly, the bottom row compares the effect of crystal rigidity, for substrates of the same curvature. Here it is also clear that for more rigid lattices [Fig. 3(d)], the crystal becomes more fractured and ribbonlike. Similar ribbonlike patterns were observed in Monte Carlo simulations of the shell formation of viral protein capsids.

To study the effects of substrate curvature and lattice rigidity, in Fig. 4 we show how the angular width θ_w , where $w = a\theta_w$, of the ribbon crystals varies with the size of the substrate (top) and the rigidity s_0 (bottom), as obtained from the simulations (black dots). This figure clearly shows that the width of the ribbonlike crystals gets smaller for higher curved substrates (smaller a) and more rigid lattices (bigger s_0).

To better understand the equilibrium width of crystals on spheres, we can approximate the free energy [Eq. (3)] for ribbonlike morphologies of width $w = a\theta_w$ and length l , as shown in Fig. 1 (see Appendix for details). The interfacial energy [first term of Eq. (3)] of a ribbon crystal on a sphere

can be approximated by

$$F_I = \int e(\nabla\phi, \Theta)|\nabla\phi|^2 dS \approx \bar{e} \left[2l \cos\left(\frac{w}{2a}\right) + 2w \right], \quad (12)$$

where $\bar{e} \approx \frac{e_0^2}{2}$ is the average of the line tension penalty. Essentially, F_I is the surface tension \bar{e} multiplied by the perimeter

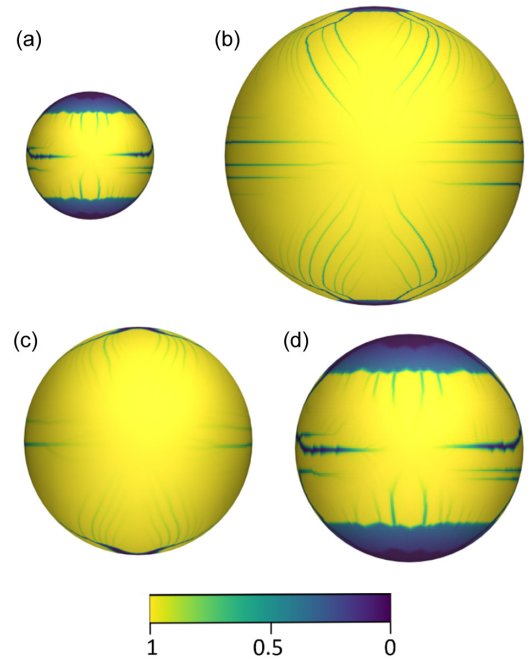


FIG. 3. Effects of substrate curvature and crystal rigidity. In the top row we compare the crystals morphologies for the same rigidity $s_0 = 0.05$ and two different substrate sizes $a = 1.5$ (a) and $a = 3.5$ (b) (the size of the figure represents the relative size of the substrate). In the bottom row we compare crystal morphologies to substrates of the same size $a = 1.5$, and the different rigidities $s_0 = 0.015$ (c) and $s_0 = 0.05$ (d).

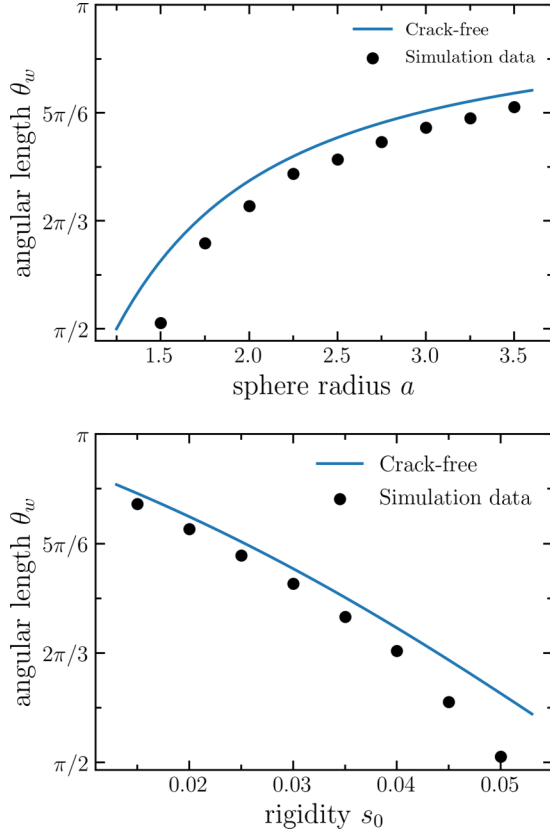


FIG. 4. Crystal angular width. These figures show the angular width of the crystal as a function of sphere radius a (top), and stiffness s_0 (bottom). The “crack-free” theoretical curve corresponds to the equilibrium angular width for a ribbon without fractures.

of the ribbon. Similarly, the bulk free energy [second term of Eq. (3)] can be approximated by

$$F_B = \int f(\phi) dS \approx -2|\Delta f| l a \sin\left(\frac{w}{2a}\right), \quad (13)$$

where $|\Delta f| = |f(\phi = 1) - f(\phi = 0)| = \frac{1}{12}$. Note that F_B is the difference between the bulk energy densities corresponding ordered and disordered phases, multiplied by the ribbon area. Finally, the elastic contribution to the free energy for a ribbon crystal can be approximated by

$$F_E = \int s_0 \phi^2 |\nabla \Theta - \Lambda| dS \approx 2l s_0 \left[1 - \cos\left(\frac{w}{2a}\right) + \sin\left(\frac{w}{2a}\right) \right], \quad (14)$$

where it is considered that for the whole crystal $\phi = 1$ and $\nabla \Theta$ vanishes in the bulk of the crystal except at the interface, where it is approximated by a δ function.

Then, the total free energy is obtained by adding the different contributions $F = F_I + F_B + F_E$. As here we have $\bar{e} \ll |\Delta f| \sim s_0$, we can obtain a first look at crystal shape considering that the energy contribution of the interface to the total free energy of the ribbon-crystal can be neglected. In this case, the equilibrium width of crystal can be obtained

by minimizing the free energy $\frac{\partial \Delta F}{\partial w} = 0$, which leads to

$$\theta_w = 2 \tan^{-1} \left(\frac{|\Delta f| a - s_0}{s_0} \right), \quad (15)$$

which approximates the width of crystals on spheres without any contribution from cracks.

Figure 4 also compares this theoretical model (corresponding to the “crack-free” label) with the results obtained from the simulations, for both, the angular width of the ribbon as a function of the sphere radius a , and rigidity s_0 . To obtain the angular width from the simulations we set $\phi = 0.5$ and averaged θ_w along the contour. Although this simple model gives a good approximation to the simulation results, Fig. 4 shows that the widths of the crystals obtained in the simulations are smaller. Note also that the deviations increase for substrates of higher curvatures (smaller sphere radius a) or stiffer crystals. This is a consequence of neglecting the interfacial free-energy contribution involved in the cracks, which was not taken into account in Eq. 15.

Regarding the cracks, Fig. 5 compares the map of the order parameter ϕ projection in the $\theta - \varphi$ spherical coordinates for a sixfold crystal growing on a sphere of radius $a = 1.5$. For the calculations we have set $s_0 = 0.01$ [Fig. 5(a)] and $s_0 = 0.05$ [Fig. 5(b)]. From these figures, it can be observed that the crystal becomes more cracked and irregular as the crystal rigidity increases. To quantify the departure from the compact shapes expected for a system without rigidity, here we calculate the degree of circularity C for crystals with different values of s_0 , as shown in Fig. 5(c). The dimensionless circularity is defined as

$$C = \frac{4\pi A}{L^2}, \quad (16)$$

where A is the total area and L is the contour length of the crystal interface. Note that the circularity of a planar circular nucleus is $C \equiv 1$, while the circularity of a fractal-like crystal approaches zero $C \equiv 0$. As the number of cracks increases, the crystal becomes more ramified, decreasing the circularity as shown in Fig. 5. Note that the circularity decreases as s_0 increases and that for large values of s_0 it approaches zero, indicating the formation of highly irregular fractal-like nuclei, similar to the patterns observed in colloidal systems [7].

IV. CONCLUSION

In this work, we have studied the effect of curvature in two-dimensional isothermal crystal growth on spherical substrates. We used Landau’s free energy expanded in a complex order parameter defining both local magnitude and crystal orientation.

As expected, the substrate’s curvature affects the shape and structure of growing crystals. As a consequence of curvature, cracks (domain walls) are produced due to curvature induced in-plane elastic strains. Note that while in classical continuum models cracks are related with singularities of the stress field around the crack tip, here we identified cracks with regions that within the time-scale of front propagation cannot crystallize due to the geometric frustration and remain in the disordered state.

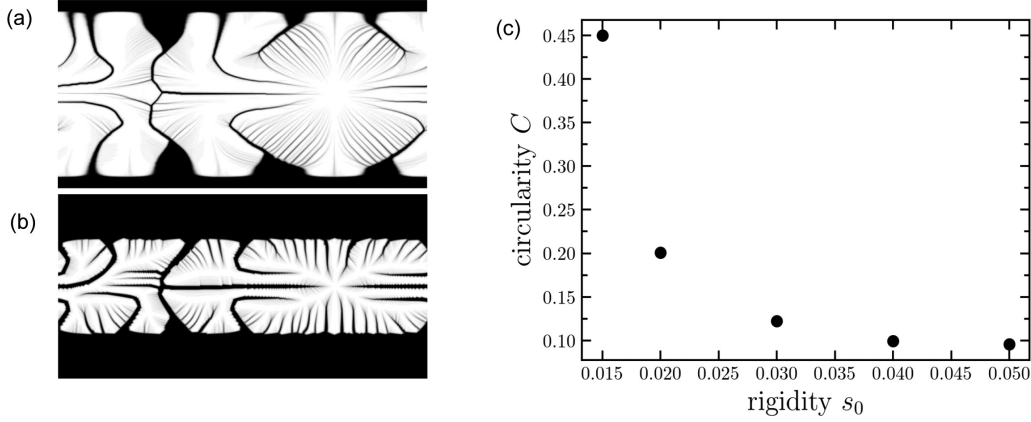


FIG. 5. Crystal cracks and dimensionless circularity. This figure shows the effect of the crystal rigidity on the geometry of crystal cracks as the crystal grows on the sphere. Panels (a, b) compare the profile of the order parameter ϕ in the $\theta - \varphi$ spherical coordinates for a sixfold crystal growing on a sphere of radius $a = 1.5$ in grayscale to denote the cracks on the crystal. In the simulation of panel (a) we have set $s_0 = 0.01$ and in panel (b) we have set $s_0 = 0.05$. Panel (c) shows the dimensionless circularity [Eq. (16)] for different values of s_0 .

For small spherical substrates (or hard lattices) initial isotropic nuclei adopt a cracked ribbonlike morphology. We derived an expression for the leading factors that controls the geometry of the crystals. Despite its simplicity, the model captures the leading parameters that dictates the role of elastic frustration in crystals growing on spheres.

ACKNOWLEDGMENTS

This work was supported by the National Research Council of Argentina, CONICET, the Fondo para la Investigación Científica y Tecnológica (FONCYT, Grant No. PICT-2017-3611), and Universidad Nacional del Sur. L.R.G. acknowledges support from the Alexander von Humboldt Foundation through the Georg Forster and return fellowships.

APPENDIX

In the crystal phase, the model studied here leads to $\phi \sim 1$ and $\nabla\Theta \sim 0$. For a circular homogeneous crystal that has a radius R , on the surface of a sphere of radius a , such as $R \ll a$, the interface energy can be approximated by energy of a planar circular crystal, i.e., $F_I \approx 2\pi\gamma R$. Similarly, the bulk energy is given by $F_B \approx \pi\Delta f R^2$. By adding to these values the elastic energy of the circular cap [Eq. (10)], the total free energy is obtained as $F_{\text{cap}} = 2\pi R\gamma - \pi R^2\Delta f + \frac{2\pi}{3}s_0\frac{R^3}{a^2}$. Then, R_{eq} is simply calculated by minimizing this free energy of the crystal cap.

For a defect-free ribbonlike crystal on a sphere of radius a , we can approximate the interface energy F_I in spherical coordinates as

$$F_I = \int_{\theta_1}^{\theta_2} \int_0^{\Delta\varphi} e(\alpha) |\nabla\phi|^2 a^2 \sin(\theta) d\varphi d\theta, \quad (17)$$

where θ_1 and θ_2 is the top and bottom polar angle of the interface of the ribbonlike crystal, respectively, while $\Delta\varphi$ represents the angular length of the crystal, as shown in Fig. 1. The parameter $e(\alpha)$ can be approximated by the mean value defined as $\bar{e} = \frac{1}{2\pi/n} \int_{-\pi/n}^{\pi/n} \frac{1}{2} \{e_0 [1 + \delta_0 \cos(n\alpha)]\}^2 d\alpha =$

$\frac{e_0^2}{4\pi/n} \frac{\pi}{n} (2 + \delta_0^2)$. For the parameters employed in this paper we have $1 \gg \delta_0^2$; therefore, $\bar{e} \sim \frac{e_0^2}{2}$.

Since $\nabla\phi$ vanishes throughout the crystal except at the interface, we can express F_I as the as a line tension \bar{e} multiplied by the perimeter of the crystal, i.e., $F_I = \bar{e} [a\Delta\varphi [\sin(\theta_2) + \sin(\theta_1)] + 2a(\theta_2 - \theta_1)]$. Finally, assuming that crystal grows symmetrically with respect to the equator axis, we can rewrite $\theta_1 = \frac{\pi}{2} - \frac{\theta_w}{2}$, $\theta_2 = \frac{\pi}{2} + \frac{\theta_w}{2}$, and let $l = a\Delta\varphi$; therefore, $F_I \approx \bar{e} [2a\Delta\varphi \cos(\frac{\theta_w}{2}) + 2a\theta_w] = \bar{e} [2l \cos(\frac{w}{2a}) + 2w]$.

The second term of the free-energy integral can be expressed in spherical coordinates as

$$F_B = \int_{\theta_1}^{\theta_2} \int_0^{\Delta\varphi} f(\phi) a^2 \sin(\theta) d\theta d\varphi. \quad (18)$$

Since $\phi \sim 1$ in the bulk of the crystal, we can take it outside the integral $F_B \approx f(\phi = 1) \int dS$ and since $f(\phi = 1) = -|\Delta f| = -|f(\phi = 1) - f(\phi = 0)|$ we obtain $F_B = -|\Delta f| \int_{\theta_1}^{\theta_2} \int_0^{\Delta\varphi} a^2 \sin(\theta) d\theta d\varphi$. After integration and replacing the angles as a function of θ_w we obtain $F_B \approx -|\Delta f| a^2 \Delta\varphi 2 \sin(\frac{\theta_w}{2}) = -2|\Delta f| l a \sin(\frac{w}{2a})$.

Finally, the third term of the free energy can be expressed in spherical coordinates as

$$F_E = \int_{\theta_1}^{\theta_2} \int_0^{\Delta\varphi} s_0 \phi^2 |\nabla\Theta - \frac{\cot(\theta)}{a} \hat{\mathbf{e}}_\varphi|^2 a^2 \sin(\theta) d\theta d\varphi. \quad (19)$$

Due to the assumptions described above, in the bulk of the crystal, we can approximate the integral to $F_E \approx s_0 a \Delta\varphi \int_{\theta_1}^{\theta_2} |\cot(\theta)| \sin(\theta) d\theta d\varphi = a s_0 \Delta\varphi 2 [1 - \cos(\frac{\theta_w}{2})] = l s_0 2 [1 - \cos(\frac{w}{2a})]$. However, since $\nabla\Theta$ vanishes in the whole crystal except for the interface, we must add to the above expression the energy evaluated at the boundaries. For simplicity, we only consider the interfaces at θ_1 and θ_2 and $\phi \sim 1$. Then, at the interface, $F_B \approx a s_0 [\int_0^{\Delta\varphi} |\cot(\theta_1)| \sin(\theta_1) d\varphi + \int_0^{\Delta\varphi} |\cot(\theta_2)| \sin(\theta_2) d\varphi] = 2 s_0 \Delta\varphi a \sin(\frac{\theta_w}{2}) = 2 s_0 l \sin(\frac{w}{2a})$. Finally, adding the two terms together gives the energy of the third term of the free energy $F_B \approx 2 \Delta\varphi a s_0 [1 - \cos(\frac{\theta_w}{2}) + \sin(\frac{\theta_w}{2})] = 2 l s_0 [1 - \cos(\frac{w}{2a}) + \sin(\frac{w}{2a})]$.

- [1] D. Kashchiev, *Nucleation: Basic Theory with Applications* (Butterworth—Heinemann, Oxford, 2000).
- [2] K. Kelton and A. L. Greer, *Nucleation in Condensed Matter: Applications in Materials and Biology*, Vol. 15 (Elsevier, Amsterdam, The Netherlands, 2010).
- [3] L. R. Gómez, N. A. García, V. Vitelli, J. Lorenzana, and D. A. Vega, Phase nucleation in curved space, *Nat. Commun.* **6**, 6856 (2015).
- [4] V. Vitelli, J. B. Lucks, and D. R. Nelson, Crystallography on curved surfaces, *Proc. Natl. Acad. Sci. USA* **103**, 12323 (2006).
- [5] G. M. Grason, Perspective: Geometrically frustrated assemblies, *J. Chem. Phys.* **145**, 110901 (2016).
- [6] S. Schneider and G. Gompper, Shapes of crystalline domains on spherical fluid vesicles, *Europhys. Lett.* **70**, 136 (2005).
- [7] G. Meng, J. Paulose, D. R. Nelson, and V. N. Manoharan, Elastic instability of a crystal growing on a curved surface, *Science* **343**, 634 (2014).
- [8] S. Armon, H. Aharoni, M. Moshe, and E. Sharon, Shape selection in chiral ribbons: From seed pods to supramolecular assemblies, *Soft Matter* **10**, 2733 (2014).
- [9] S. Li, R. Zandi, A. Travasset, and G. M. Grason, Ground States of Crystalline Caps: Generalized Jellium on Curved Space, *Phys. Rev. Lett.* **123**, 145501 (2019).
- [10] N. A. García, A. D. Pezzutti, R. A. Register, D. A. Vega, and L. R. Gómez, Defect formation and coarsening in hexagonal 2D curved crystals, *Soft Matter* **11**, 898 (2015).
- [11] S. Panahandeh, S. Li, L. Marichal, R. Leite Rubim, G. Tresset, and R. Zandi, How a virus circumvents energy barriers to form symmetric shells, *ACS Nano* **14**, 3170 (2020).
- [12] C. Köhler, R. Backofen, and A. Voigt, Stress-Induced Branching of Growing Crystals on Curved Surfaces, *Phys. Rev. Lett.* **116**, 135502 (2016).
- [13] L. Ortellado and L. R. Gómez, Phase field modeling of dendritic growth on spherical surfaces, *Front. Mater.* **7**, 163 (2020).
- [14] P. Toledano and J.-c. Toledano, *Landau Theory of Phase Transitions: The Application to Structural, Incommensurate, Magnetic, and Liquid Crystal Systems*, Vol. 3 (World Scientific, Singapore, 1987), p. 5.
- [15] S.-K. Chan, Steady-state kinetics of diffusionless first-order phase transformations, *J. Chem. Phys.* **67**, 5755 (1977).
- [16] J. A. Warren, R. Kobayashi, A. E. Lobkovsky, and W. C. Carter, Extending phase field models of solidification to polycrystalline materials, *Acta Mater.* **51**, 6035 (2003).
- [17] H. Yu, N. Gupta, Z. Hu, K. Wang, B. R. Srijanto, K. Xiao, D. B. Geohegan, and B. I. Yakobson, Tilt grain boundary topology induced by substrate topography, *ACS Nano* **11**, 8612 (2017).
- [18] B. O'Neill, *Elementary Differential Geometry* (Academic Press, San Diego, 1997).
- [19] R. Kobayashi, J. A. Warren, and W. C. Carter, A continuum model of grain boundaries, *Physica D* **140**, 141 (2000).
- [20] N. Provatas and K. Elder, *Phase-field Methods in Materials Science and Engineering* (John Wiley & Sons, New York, 2011).
- [21] K. R. Elder, M. Katakowski, M. Haataja, and M. Grant, Modeling Elasticity in Crystal Growth, *Phys. Rev. Lett.* **88**, 245701 (2002).
- [22] L. R. Gómez, E. M. Vallés, and D. A. Vega, Lifshitz-Safran Coarsening Dynamics In a 2D Hexagonal System, *Phys. Rev. Lett.* **97**, 188302 (2006).
- [23] E. Alster, K. R. Elder, J. J. Hoyt, and P. W. Voorhees, Phase-field-crystal model for ordered crystals, *Phys. Rev. E* **95**, 022105 (2017).
- [24] R. Kobayashi, Modeling and numerical simulations of dendritic crystal growth, *Physica D* **63**, 410 (1993).
- [25] C. I. Mendoza and D. Reguera, Shape selection and misassembly in viral capsid formation by elastic frustration, *eLife* **9**, e52525 (2020).
- [26] See Supplemental Material at <http://link.aps.org/supplemental/10.1103/PhysRevE.105.014801> for movies of the growth of crystals on the surface of a sphere.
- [27] N. P. Mitchell, R. L. Carey, J. Hannah, Y. Wang, M. Cortes Ruiz, S. P. McBride, X. M. Lin, and H. M. Jaeger, Conforming nanoparticle sheets to surfaces with Gaussian curvature, *Soft Matter* **14**, 9107 (2018).